Birck and NCN Publications   Birck Nanotechnology Center

4-2010

Fabrication of conductive interconnects by Ag migration in Cu-Ag core-shell nanoparticles

Suk Jun Kim
Purdue University - Main Campus

E A. Stach
Birck Nanotechnology Center and School of Materials Engineering, Purdue University, eastach@purdue.edu

Carol A. Handwerker
Purdue University - Main Campus, handwerker@purdue.edu

Follow this and additional works at: http://docs.lib.purdue.edu/nanopub
Part of the Nanoscience and Nanotechnology Commons

Fabrication of conductive interconnects by Ag migration in Cu–Ag core-shell nanoparticles

Suk Jun Kim, Eric A. Stach, and Carol A. Handwerker[a)]

School of Materials Engineering and Birck Nanotechnology Center, Purdue University, West Lafayette, Indiana 47907, USA

Fabrication of conductive nanoparticle films is observed in Cu–Ag core-shell nanoparticles by fast diffusion of Ag at 220 °C from particle surfaces, leading to the formation of sintered necks of Ag at the initial particle-particle contacts. Transmission electron microscopy showed that the necks were pure Ag and that particle surfaces away from the contacts were nearly Ag-free. The extent of neck formation is controllable by the choice of initial Ag thickness. Analysis of the thermodynamics of the Ag–Cu system and the relative diffusivities of Ag and Cu provide criteria for fabrication of other core-shell two-phase systems by the same mechanism. © *2010 American Institute of Physics*. [doi:10.1063/1.3364132]

With the EU (European Union) and Chinese bans of Pb–Sn eutectic solder for electronic interconnects, the microelectronics research community has been examining a range of possible Pb-free alternatives for interconnection, even nonsolder based technologies.[1,2] The dominant Pb-free solders currently used in high-volume consumer electronics are near eutectic Sn–Ag–Cu alloys, with some use of Sn–Cu alloys with ternary additions to modify wetting and interactions with substrate materials.[3–5] Although consumer electronics have transitioned almost entirely to Pb-free solder interconnects, the interconnects still have poorer drop/impact behavior and higher processing temperatures (240 °C) compared with Sn–Pb eutectic (220 °C). In addition, their highly anisotropic solidification, thermal expansion, and mechanical behavior have left the microelectronics industry looking for improved interconnect solutions, including those not involving solder.[6]

Here we report on a solderless interconnect fabrication process based on the low temperature sintering of Cu–Ag core-shell nanoparticles to form porous, conductive structures. This interconnect fabrication process has the potential to replace traditional soldering in some applications, as well as replacing high-Pb and Au-containing solder alloys used for high temperature die attach of semiconductor devices.

Nanoparticles of Cu were fabricated and then coated with Ag to form core-shell Cu–Ag (10 wt % Ag) nanoparticles,[7] and the particle diameters were 460 ± 110 nm (Cu particles) and 470 ± 110 nm (Cu–Ag) (N=200).[8] The calculated Ag shell thickness is approximately 7 nm with an assumption of 470 nm diameter spherical particles and uniform shell thickness. Pressed powder compacts (1 g) were formed from each of the particle types using a 3/4 inch-diameter die under 78 MPa for 30 s. The resulting porous compacts were inverted within the die and pressed once more under the same pressure for the same duration. The compacts were heated in argon from room temperature at a heating rate of 4 °C/min to 220 °C and held at 220 °C for 10 min. Compact density before and after sintering was determined using careful measurements of the

dimensions of the compacts. The average grain size was determined by x-ray diffraction (XRD, Bruker D8 Focus) measurements via Scherrer's formula using the (111) peaks of Ag and Cu with the peak width calibrated with Al_2O_3 from the National Institute of Standards and Technology Standard Reference Material (NIST SRM) 676a. The microstructures of particle-particle contacts were determined from fracture surfaces examined by scanning electron microscopy (SEM–Hitachi S-4800). For transmission electron microscopy (TEM) analysis, epoxy (Allied, EpoxyBond 110™) was applied to the surface of un-annealed and annealed compacts, allowed to infiltrate the pores, and cured at 130 °C for 10 min in air. The compacts were subsequently polished following conventional bulk TEM sample preparation methods.[9] Characterization by TEM and energy-filtered TEM (EFTEM) was performed using an FEI Titan 80/300.

From examination of the fracture surfaces (Fig. 1), the pure Cu compacts showed no appreciable interparticle contact formation for either the as-received particles or after annealing at 220 °C. For the Cu–Ag nanoparticles, powder compacts of the as-received nanoparticles showed occasional
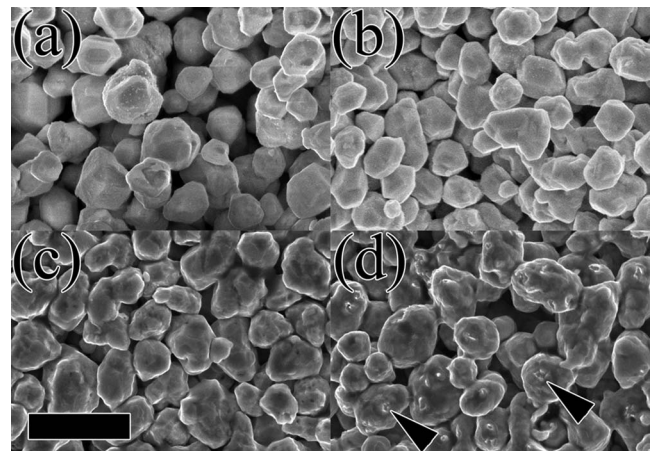

FIG. 1. SEM cross-sectional images of the compacts before [(a) and (c)] after [(b) and (d)] annealing at 220 °C: (a) and (b) pure Cu nanoparticle compacts and (c) and (d) Cu–Ag nanoparticle compacts. The arrows in (d) indicate fractured necks which are evidence of significant sintering. Scale bar is 1 μm.

a)Author to whom correspondence should be addressed. Electronic mail: handwerker@purdue.edu.

96, 144101-1

TABLE I. Relative density and grain size comparison between Cu and Cu–Ag particle compact before and after annealing at 220 °C.

	Cu compact before annealing	Cu compact after annealing	Cu–Ag compact before annealing	Cu–Ag compact after annealing
Relative density	0.53 ± 0.01	0.56	0.50 ± 0.01	0.70
Cu grain size (nm)	89 ± 9	114 ± 14	107 ± 5	104 ± 5
Ag grain size (nm)	NA	NA	[a]	23 ± 3

[a]Ag peak intensity too weak for analysis.

interparticle contact formed during the Ag deposition process. However, after annealing at 220 °C, a significant number of interparticle contacts were evident from the occurrence of fractured "necks," where particle-particle sintering had occurred.[10]

Table I summarizes the effects of interparticle sintering on the density and grain size of the Cu and Ag particles as estimated from XRD. Because the measurement error in the compact thickness is lower than the error in diameter, the density of compacts before annealing was calculated based on physical measurement, while the density of compacts after annealing was calculated with the volume estimated using the relationship between volume shrinkage and linear shrinkage.

$$\frac{\Delta V}{V_0} = 1 - \left(1 - \frac{\Delta L}{L_0}\right)^3, \qquad (1)$$

where V is volume and L is pellet thickness. These measurements indicate that densification and Ag grain growth occurred in Cu–Ag while little densification was observed in pure Cu. There was no apparent change in the Cu grain size within the Cu–Ag particles with annealing. However, it should be noted that the full width at half maximum of the XRD peak of Ag before annealing was unmeasurable due to its low intensity. After annealing, the intensity of the Ag XRD peaks increased due to the formation of sintered Ag necks at particle-particle contacts, leading to a calculated Ag grain size of 23 nm.

The above data indicates that there is a significant difference between the sintering behavior of pure Cu and the Cu–Ag core-shell nanoparticles. TEM and EFTEM were used to investigate the effect of the Ag layer on interparticle sintering, to determine the microstructural origins of the above response.[11] The Ag jump ratio map was obtained using a 20 eV energy-selection slit, with a slit position of 367 eV for the pre-edge image and 410 eV for the postedge image and an exposure time of 30 s. The Cu elemental map was obtained using two pre-edge windows (centered at 865 and 895 eV) and a postedge window centered at 970 eV, each with a 30 eV slit width and an exposure time of 30 s. Because the low concentration of Ag results in a noisy elemental map, the Ag layer was characterized using the jump ratio technique.[12,13] As shown in Fig. 2(b), the Cu–Ag particles are coated with a relatively uniform Ag layer prior to annealing. The Cu elemental map in Fig. 2(c) precludes the possibility that the contrast in Fig. 2(b) was caused by misalignment of pre-edge and postedge. The higher magnification image [Fig. 2(d)] supports this interpretation, as the Ag layer exhibits a difference in contrast related to its different composition and crystalline orientation. The average thickness of Ag shell was estimated by TEM from measurements of cross

sections of particles whose diameters were close to the average particle (470 nm). The measured thickness is 8 ± 3 nm (N=50) which is comparable to 7 nm, the calculated value. Some variation in the Ag shell thickness with surface facet orientation may occur due to the different preference of Ag adatom attachment on different Cu facets, as reported by Baletto et al.[14]

The effect of Ag diffusion on interparticle sintering is examined in Fig. 3. The bright field micrograph shown as Fig. 3(a) clearly indicates both enhanced interparticle sintering and a less faceted morphology following annealing compared with Fig. 2(a). The EFTEM images of Figs. 3(b)–3(d) demonstrate that Ag that was originally present in the shell of the core-shell nanoparticles has diffused from the surfaces to the particle-particle contacts. The observation of neck formation by Ag diffusion and segregation during interparticle sintering at a temperature as low as 220 °C with little interdiffusion is consistent with the low solubility of Ag in Cu and Cu in Ag at these temperatures, consistent with the Ag–Cu binary phase diagram.[15]

Other systems that may display preferential sintering by surface diffusion of the shell atoms to the particle-particle contacts are (1) binary eutectic systems with limited solid solubility at the annealing temperatures and (2) those that
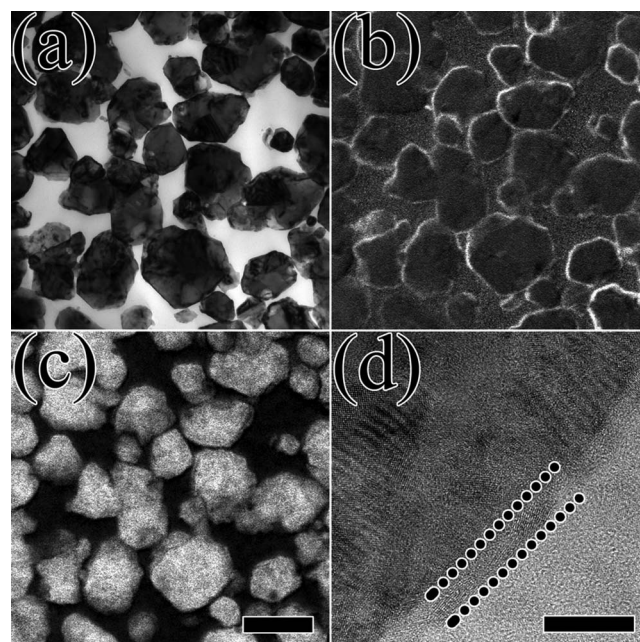

FIG. 2. TEM and EFTEM images of the Cu–Ag particle compact before annealing: (a) TEM image, (b) Ag jump ratio map image of (a) area, (c) Cu elemental map image (a) area, (d) particle surface area at high magnification; Ag layer is indicated by two parallel dashed lines. The scale bar: 500 nm in (c) and 10 nm in (d).
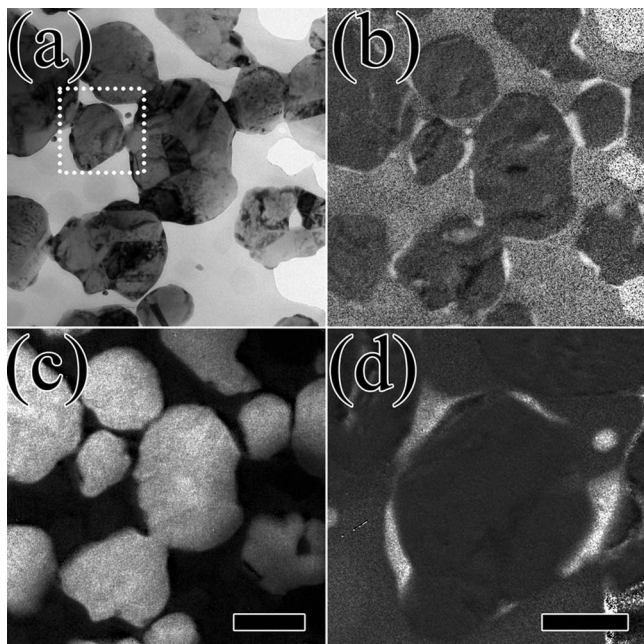
FIG. 3. TEM and EFTEM images of the Cu–Ag compact after annealing at 220 °C: (a) TEM image, (b) Ag ratio map of (a) area, (c) Cu elemental map of (a) area, (d) Ag ratio map of white box area in (a). The scale bar: 300 nm in (c) and 100 nm in (d).

have significantly faster surface diffusion of the shell phase than the core phase. For the Ag–Cu system examined here, we can calculate an effective surface diffusion coefficient (D_S) using Eq. (2) based on neck formation by surface diffusion.[16,17]

$$x^7 = \frac{56 D_S \delta_S \gamma_S V_m a^3}{RT} t, \qquad (2)$$

where x: observed neck radius, 50×10^{-9} m, D_S: surface diffusion coefficient, δ_S: diffusion layer thickness typical for surface diffusion, assumed to be 0.5×10^{-9} m, γ_S: surface energy, 1.2 J/m^2,[18] V_m: molar volume, 1.027×10^{-5} m^3/mol, a: particle radius, 235×10^{-9} m based on average Cu–Ag particle radius, t: time, R: gas constant, 8.314 J/mol K, and T: sintering temperature, 493 K. The effective surface diffusion coefficient for 493 K can be bounded using the total annealing time including the temperature ramp of 3.6×10^3 s and the 600 s hold at 493 K, corresponding to 2.0×10^{-19}–1.3×10^{-18} m^2/s, respectively. This range is in good agreement with the surface diffusivity, 1.4×10^{-19} m^2/s, measured by Dannenberg et al.[19] at similar temperatures and annealing atmosphere.

If the surface diffusion of Cu in our experiments was broadly similar to that of Ag, we would expect to find 40–70 nm radius necks in the pure Cu nanoparticles [based on Eq. (2) with γ_S: 1.8 J/m^2, V_m: 7.11×10^{-6} m^3/mol, a: 230×10^{-9} m for Cu particles]. This was not observed, indicating that the surface diffusion of Ag ($\sim 10^{-19}$ m^2/s) was much faster than that of Cu (we estimate an upper bound of $\sim 10^{-23}$ m^2/s for Cu, based our minimum detectable size of ~ 10 nm). One might expect the surface self diffusion coefficients for Cu and Ag to be similar (based on similarities in melting temperature and crystal structure), but wide ranges of surface diffusion coefficients have been reported

in the literature for Ag on Cu (10^{-12}–10^{-9} m^2/s),[20] Ag (10^{-32}–10^{-9} m^2/s),[19–23] and Cu (10^{-22}–10^{-16} m^2/s) (Refs. 16 and 23–25) at 493 K. The observed difference between Ag and Cu self-diffusion is therefore not entirely unexpected.

The results presented in this paper suggest that sintering of Cu–Ag core-shell nanoparticles is a promising nanotechnology-based process for producing Pb-free solderless interconnects when the surface self diffusivity of the shell phase is significantly faster than that of the core phase at the temperatures of interest. Substantial neck formation combined with little shrinkage leads to dimensionally stable interconnects. The extent of neck formation and thus, the final microstructure, can be controlled by the thickness of the initial Ag shell phase, with the driving force for diffusion controlled by the overall particle size. Despite the promising thermal stability reported herein, it will be crucial to determine the mechanical properties of these systems with respect to strength and resistance to failure by drop/shock to adequately assess their suitability as Pb-free solder replacements.

[1] K. N. Tu, A. M. Gusak, and M. Li, J. Appl. Phys. **93**, 1335 (2003).
[2] P. Borgesen, T. Bieler, L. P. Lehman, and E. J. Cotts, MRS Bull. **32**, 360 (2007).
[3] K. W. Moon, W. J. Boettinger, U. R. Kattner, F. S. Biancaniello, and C. A. Handwerker, J. Electron. Mater. **29**, 1122 (2000).
[4] W. Yang, R. W. Messler, and L. E. Felton, J. Electron. Mater. **23**, 765 (1994).
[5] W. J. Boettinger, C. E. Johnson, L. A. Bendersky, K. W. Moon, M. E. Williams, and G. R. Stafford, Acta Mater. **53**, 5033 (2005).
[6] S. Choi, K. N. Subramanian, J. P. Lucas, and T. R. Bieler, J. Electron. Mater. **29**, 1249 (2000).
[7] Ames Goldsmith, South Glenn Falls, New York.
[8] S. J. Dapkunas, A. Jillavenkatesa, and L. H. Lum, *Particle Size Characterization* (NIST, Gaithersburg, MD 2001).
[9] P. J. Goodhew, *Specimen Preparation for Transmission Electron Microscopy of Materials* (Oxford University Press, Oxford, UK, 1984).
[10] M. F. Ashby, Acta Metall. **22**, 275 (1974).
[11] D. B. Williams and C. B. Carter, *Transmission Electron Microscopy – A Textbook for Materials Science* (Plenum, New York, 1996).
[12] F. Hofer and P. Warbichler, Ultramicroscopy **63**, 21 (1996).
[13] F. Hofer, W. Grogger, G. Kothleitner, and P. Warbichler, Ultramicroscopy **67**, 83 (1997).
[14] F. Baletto, C. Mottet, and R. Ferrando, Phys. Rev. B **66**, 155420 (2002).
[15] *ASM Binary Alloy Phase diagrams*, 2nd Edition, T. B. Massalski, H. Okamoto (ASM International, Materials Park, Ohio 1990).
[16] G. C. Kuczynski, Trans. Metall. Soc. AIME **185**, 169 (1949).
[17] S. J. Kang, *Sintering Densification, Grain Growth & Microstructure* (Elsevier Butterworth-Heinemann, Oxford, 2005).
[18] J. M. Howe, *Interfaces in Materials* (Wiley, New York, 1997).
[19] R. Dannenberg, E. A. Stach, J. R. Groza, and B. J. Dresser, Thin Solid Films **370**, 54 (2000).
[20] U. Kurpick, G. Meister, and A. Goldmann, Appl. Surf. Sci. **89**, 383 (1995).
[21] G. E. Rhead, Acta Metall. **13**, 223 (1965).
[22] K. Yoshihara and K. Nii, Trans. Jpn. Inst. Met. **20**, 533 (1979).
[23] R. R. Hough, Scripta Metallurgica **4**, 559 (1970).
[24] J. Y. Choi and P. G. Shewmon, Trans. Metall. Soc. AIME **224**, 589 (1962).
[25] N. A. Gjostein, Trans. Metall. Soc. AIME **221**, 1039 (1961).